Received 25 March 2023; accepted 9 May 2023. Date of publication 12 May 2023; date of current version 1 June 2023.

Digital Object Identifier 10.1109/OJUFFC.2023.3275936

Pulsing and Detection Strategies for Contrast-Enhanced Ultrasound: A Narrative Review

SAPNA R. BISHT[1], VISHWAS V. TRIVEDI[2], ROHIT BHARDWAJ[3], CHANDAN K. JHA[2], DEBABRATA GHOSH[3] (Member, IEEE), AND HIMANSHU SHEKHAR[2] (Senior Member, IEEE)

[1]Discipline of Biological Engineering, Indian Institute of Technology (IIT) Gandhinagar, Gandhinagar, Gujarat 382355, India
[2]Discipline of Electrical Engineering, Indian Institute of Technology (IIT) Gandhinagar, Gandhinagar, Gujarat 382355, India
[3]Department of Electronics and Communication Engineering, Thapar Institute of Technology, Patiala, Punjab 147004, India

CORRESPONDING AUTHOR: H. SHEKHAR (himanshu.shekhar@iitgn.ac.in)

This work was supported by Science and Engineering Research Board, Government of India through grant # SRG/2020/001123.

ABSTRACT Contrast-enhanced imaging has grown significantly in the past two decades. Technology has evolved from imaging based on linear principles to elaborate pulsing and microbubble-specific detection strategies. This review provides a broad overview of the research published on these topics, emphasizing the progress made, current challenges, and future research considerations. We cover the physical and conceptual underpinnings of imaging based on ultrasound contrast agents, focused on pulsing and detection strategies. The techniques proposed are categorized according to the underlying fundamental physical and signal processing principles. We revisit methods that were previously only of academic interest and may now be clinically feasible with advances in computation and hardware. We discuss unmet challenges and opportunities originating from developments in other sub-fields of ultrasound imaging to enable wider clinical adoption of contrast-enhanced ultrasound.

INDEX TERMS Contrast-enhanced ultrasound, pulsing strategies, nonlinear imaging, contrast agent detection.

I. INTRODUCTION

CONTRAST-ENHANCED ultrasound (CEUS) imaging is an essential tool for diagnostic radiology available for clinical indications in the USA, Europe, and Asia [1], [2]. Previously reported articles detail the evolution of ultrasound contrast agents, their chemical composition, clinical indications, and current status [3], [4], [5], [6], [7], [8], [9], [10]. The physical understanding of the interaction of contrast agents with ultrasound (US) has evolved in the past decade, improving CEUS methods. Recent research on CEUS has focused on nonlinear signal detection. Specifically, contrast-specific imaging techniques such as second harmonic, pulse inversion, amplitude modulation, and harmonic power Doppler are now available in the clinic [1].

A large number of techniques reported are not available commercially because of technological and economic reasons. Given recent technological developments, a renewed focus on previously reported techniques is of interest. The objective of this narrative review is twofold. First, to provide a holistic view of the research in this area, focusing on current challenges and research considerations to enable technological progress and clinical adoption. The second objective is to lower the barrier of entry for new researchers in CEUS. Specifically, we focus on the conceptual basis and signal processing aspects of imaging based on ultrasound contrast agents (UCA), emphasizing pulsing and detection strategies. Three articles with a similar scope were published nearly two decades ago [11], [12], [13]. However, the field has advanced significantly since then. Detailed reviews have appeared on specialized topics such as super-resolution imaging [14]. A recent in-depth review by Averkiou and colleagues emphasizes clinical and instrumentation aspects of CEUS imaging, and discusses selected techniques that are already in clinical use or on the horizon [1]. The present study focuses on complementary topics and discusses largely a different set of articles. Specifically, we emphasize pulsing

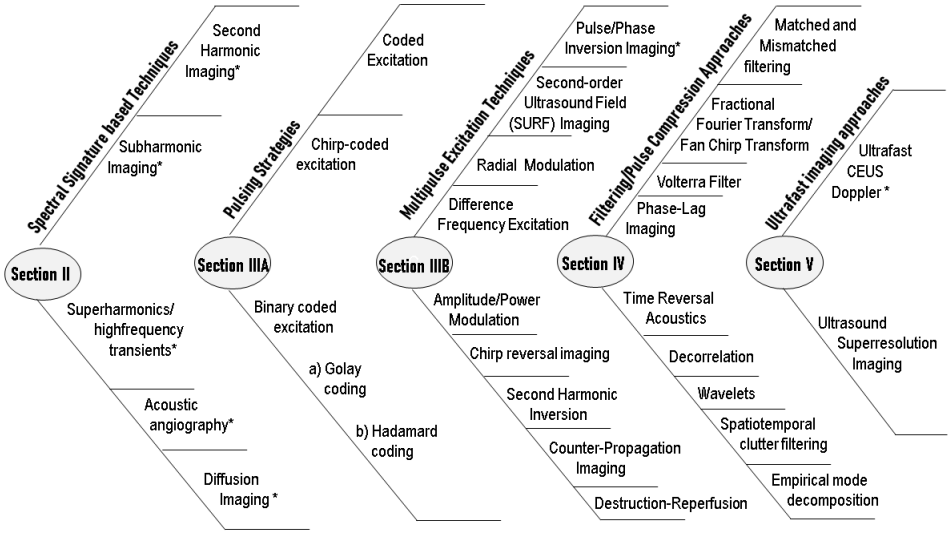

FIGURE 1. Categorization of pulsing and detection strategies for contrast-enhanced ultrasound (CEUS) imaging. ∗ Commercially available technique.

and detection strategies in the context of signal processing. This article is organized as follows (Fig. 1): Section II discusses unique acoustic signatures of microbubbles and imaging techniques that exploit them. Section III comprises of (A) pulsing and (B) multipulse excitation techniques. Section IV discusses signal processing techniques related to filtering and pulse compression.

II. SPECTRAL SIGNATURE-BASED TECHNIQUES

A. SECOND HARMONIC IMAGING

Second harmonic imaging was the first reported nonlinear CEUS imaging mode [15]. Harmonics are generated both by UCA and by tissue due to the UCA's nonlinear oscillation and nonlinear propagation in tissue, respectively. However, the harmonics from UCAs are typically stronger than those from tissue due to the relatively large nonlinearity of the microbubbles compared to tissue for insonation at low MI [16]. Imaging is typically performed with low transmit pressures (50 kPa – a few hundred kPa) and low transmit frequencies (1.5 – 3 MHz) [11], [12], [13] to reduce tissue harmonics. Second harmonic imaging is widely available on commercial systems [1]. It provides higher resolution due to the higher frequency of imaging compared to the transmitted signal. However, at high pressures and frequencies, nonlinear propagation is significant, which reduces contrast-to-tisse ratio (CTR) [17], [18]. The imaging depth is limited due to the higher attenuation of the harmonic component. Harmonic imaging has also been reported at high transmission frequencies for Intravascular Ultrasound (IVUS) imaging (greater than 10 MHz) [19].

B. SUBHARMONIC IMAGING

Subharmonic imaging offers a high CTR because tissues do not generate appreciable subharmonic signal. The insonation pressure should exceed a threshold to observe a subharmonic response, which depends on acoustic pulse parameters [20], [21], [22], [23], [24] and the physical properties of UCA. Buckling and shell rupture contribute strongly to subharmonic and ultraharmonic generation [25]. Chirps, triangular, rectangular, and dual-frequency pulses were shown to enhance subharmonic emission and reduce its threshold [26], [27], [28]. The threshold also decreases with pulse duration and increases if the excitation pulse envelope is tapered [22], [29], [30]. However, long-duration sinusoidal signals degrade the axial resolution. Coded excitation techniques can address this limitation (Section III-A).

Subharmonic imaging achieves higher penetration depth relative to harmonic imaging (at the same transmit frequency). However, threshold behavior limits sensitivity, especially for deeper locations. Further, subharmonic imaging is limited by the transducer bandwidth. The subharmonic response of UCA has a strong size dependence [20], [31]. Daeichin et al. reported a comparison of subharmonic (SH), nonlinear fundamental (NF), and ultraharmonic (UH) imaging [32]. They combined multipulse techniques (section III-B) – pulse inversion (PI), amplitude modulation (AM), and a combination of PI and AM (PIAM) along with SH, NF, and UH imaging. Subharmonic imaging had the best performance at limited (8 mm) depth than NF and UH imaging. The combination of SH/PI had the highest CTR at 8 mm depth. At a depth of 16 mm, NF showed the best performance. With a bandlimited transducer, UH imaging achieved better performance than SH imaging [33]. Further, UH and SH modes can be combined [34]. Figure 2 compares fundamental, SH, UH, and combined modes for IVUS.

Subharmonic imaging was reported for small and large animal imaging [35], [36]. Goertz et al. used SH imaging at 30 MHz transmit frequency to resolve submillimeter vessels in rabbits [35]. Subharmonic imaging was also performed in canines [37] and in breast cancer patients [36].

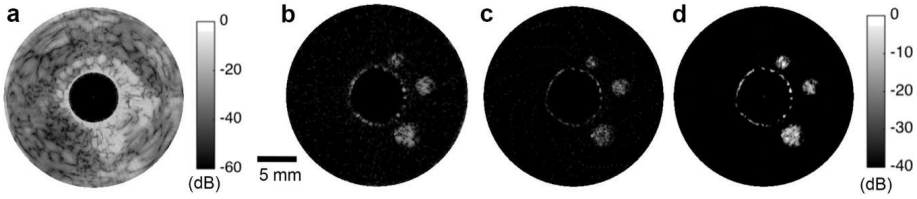

FIGURE 2. Comparison of (a) fundamental, (b) subharmonic, (c) ultraharmonic and (d) combined-mode images acquired at 12-MHz with a peripheral imaging catheter. The phantom contains 3 flow channels along with the main lumen. The flow channels were not visible in the fundamental images (a) but were clearly visible in nonlinear images (b, c and d). Reprinted from Ultrasound in Medicine & Biology, Volume 43, Issue 11, November 2017, H. Shekhar, J. S. Rowan, M. M. Doyley, "Combining Subharmonic and Ultraharmonic Modes for Intravascular Ultrasound Imaging: A Preliminary Evaluation", Pages 2725-2732, Copyright (2017), with permission from Elsevier.

Forsberg et al. imaged breast lesions using 3D CEUS harmonic (transmit 5 MHz, receive 10 MHz) and subharmonic imaging (transmit 5.8 MHz, receive 2.9 MHz). Combining SH imaging with clinical assessment improved the characterization of the suspicious lesion (accuracy 97%) [38]. Sridharan et al. reported 3D SH imaging of microbubble flow in breast lesions [36]. Subharmonic signals have also been used for noninvasive pressure estimation [39], [40], [41], [42]. Advances in monodisperse agents and transducer bandwidth can make SH imaging attractive for superficial depth applications.

C. SUPERHARMONICS/HIGH-FREQUENCY TRANSIENTS

Superharmonic imaging employs higher UCA harmonics (3rd, 4th, and 5th combined) [43]. It improves CTR because nonlinear propagation is relatively weaker for higher harmonics [46], [47]. Higher frequencies also enhance resolution at the cost of lower imaging depth. Low-frequency excitation used in this imaging approach causes larger microbubble expansion, which can cause microbubble fragmentation [43]. Bouakaz et al. used a wideband 96-element phased array for superharmonic imaging. This array was capable of operating at 900 kHz and 2.8 MHz [45]. Developing dual frequency transducers for such applications is an active area of research [46], [47]. Superharmonic imaging uses discrete frequency bands, which can cause ''ghost'' artifacts. van Neer et al. proposed a dual-pulse frequency compounding technique to address this limitation [48]. Two pulses with slightly different center frequencies were fired, and the received echoes compounded. The authors reported suppression of ghost artifacts and an improved resolution. However, the frame rate was reduced two-fold. Danilouchkine et al. divided the transducer's transmit aperture and used one-half to transmit at a higher frequency, and the other-half to transmit at a lower frequency [49]. Studies in flow phantoms and mitral valve leaflets showed resolution enhancement and artifact suppression without compromising the frame rate.

D. ACOUSTIC ANGIOGRAPHY

Acoustic angiography uses the high-frequency broadband response of microbubbles to visualize blood vessels with high spatial resolution [50]. It employs low frequency (1–5 MHz) pulses to generate broadband harmonic echoes from microbubbles (>10 MHz) [50]. This technique can potentially distinguish between healthy and tumor tissue based on microvessel tortuosity. Acoustic angiography was used to create a high-resolution 3D map of the microvasculature [51]. Gessner et al. used a confocal dual frequency wobbler transducer to achieve 20 dB CTR in resolving 150–200 μm vessels [50], [52], [53]. Broadband harmonic echoes exploited in acoustic angiography occur primarily due to microbubble fragmentation, which can limit sensitivity [54]. While acoustic angiography benefits from high CTR, the penetration depth is limited because of reliance on high-frequency UCA signals. The clinical applications of acoustic angiography may be limited to relatively superficial organs. The feasibility of acoustic angiography has been demonstrated in pre-clinical models [51], [55] and patients for imaging vasculature in the wrist, hand, and breast [56]. The reader is directed to [51] for a detailed review of acoustic angiography.

E. DIFFUSION IMAGING

Kuenen et al. proposed Contrast Ultrasound Diffusion Imaging [57]. Diffusion refers to spreading of the UCA in the microvasculature because of a concentration gradient. This method quantifies diffusion by measuring the image gray levels over time. Local diffusion was estimated from the modeled relationship between UCA and gray levels. Diffusion parametric images of four patients were compared with histology data. The area under the receiver operating characteristic curve (AUROC) of 0.91 was observed for prostate cancer localization in four patients [57]. Schalk et al. implemented a 3D version of this technique based on spatio-temporal analysis of 4D Dynamic Contrast-enhanced Ultrasound (DCE-US) data for prostate tumor imaging [58]. Instead of model fitting with a convective diffusion model, a spatiotemporal similarity analysis between the spatial time intensity curves (TICs) was reported to assess local dispersion kinetics [59], [60]. Mutual information as a nonlinear similarity measure between neighboring TICs has also been employed to obtain diffusion-related parameters [61].

Sloun et al. developed a method to enable the independent estimation of dispersion and velocity. The vascular network was modeled as a dynamic linear system, and its impulse response was locally estimated using the indicator-dilution curves. The dispersion coefficient and velocity were then extracted through a model-based parameter estimation approach. In a clinical study on prostate cancer localization with 25 patients, an AUROC of 0.84 was reported [62].

III. PULSING AND MULTIPULSE EXCITATION TECHNIQUES

A. PULSING STRATEGIES

CEUS techniques typically use low MI (∼0.1) [63]. Approaches based on microbubble destruction have also been reported for CEUS at higher MI [64] (also see Section III-B.9). Pulsing techniques in CEUS can be divided into two broad categories, those that (i) enhance the nonlinear response from UCA (e.g., chirp pulsing) and (ii) suppress the tissue response to enable UCA-specific detection (e.g., pulse inversion).

Coded excitation has been used widely for improving the SNR of traditional B-Mode imaging. Some coded excitation techniques have been reported to enhance the UCA signal without significantly compromising the axial resolution [21], [33]. The excitation pressure is typically limited for CEUS, necessitating SNR enhancement. Imaging modes such as subharmonic and ultra-harmonic imaging (see Section I) require longer-duration pulses. Additionally, the dynamic range used in CEUS (10–30 dB) [51] is considerably lower than conventional B-Mode imaging (∼50–80 dB). Therefore, sidelobe artifacts that are characteristic of coded-excitation may not appear prominently in CEUS.

1) CHIRP-CODED EXCITATION

Chirp-coded excitation has been reported most widely in CEUS [65], [66], [67]. Linear, quadratic, and logarithmic chirps have been explored. Nonlinear frequency modulated chirps are more sensitive to the frequency shifts due to attenuation, which can lead to artifacts when the chirps are decoded [68]. Linear frequency chirps are robust to such artifacts because of their linear group delay. Techniques such as matched filtering are used for decoding, leading to a short pulse length [67]. Chirp-coded excitation has also been used with harmonic and superharmonic imaging [65], [66], [67].

2) BINARY CODED EXCITATION

a: GOLAY CODING

Golay codes have a short correlation length, which is exploited for pulse compression using matched filtering. Pairs of sequences with the same length are employed. Summing of the individual autocorrelation functions of each Golay code pair eliminates sidelobes [69]. Leavens et al. combined Golay-based phase encoding with multipulse techniques (pulse inversion and amplitude modulation) and tested imaging performance in vitro [70]. A 6.5-dB improvement was reported versus conventional multipulse excitation. Shen and Shi employed Golay encoding and 3f0 (three times the frequency of insonation) transmit phasing to enhance the SNR of CEUS [71]. Although SNR was enhanced, range sidelobes were observed. These codes involve sharp changes in the phase of the transmitted waveform, and therefore, are limited by transducer bandwidth. Additionally, this approach requires one transmission each for the code pair's two signals, reducing frame rate and introducing potential motion artifacts.

b: HADAMARD CODING

Gong et al. proposed Hadamard-encoded multipulses (HEM) with fundamental frequency bandpass filtering to improve the CTR and SNR [72]. Multipulses encoded with a second-order Hadamard matrix were sequentially emitted in each of the two transmission events. Fundamental band-pass filtering was performed on the received echoes to suppress residual tissue-related second-order harmonics. Next, Hadamard decoding was performed on the filtered RF echoes, and the decoded RF signals were aligned and subtracted from each other to obtain the nonlinear fundamental energy. Nearly 20 dB CTR was achieved in vitro. Gong et al. combined fourth-order HEM pulse with multiplane wave imaging to further enhance SNR and CTR [73]. Despite substantial SNR and CTR improvement, HEM can degrade spatial resolution. Fourth-order Hadamard decoding was combined with orthogonal decoding and pulse-inversion to improve CTR by 5.4 dB [74].

B. MULTIPULSE EXCITATION TECHNIQUES

For a detailed discussion on commonly used multipulse techniques, the reader is directed to Averkiou [1] and Crocco [75].

1) PULSE/PHASE INVERSION IMAGING

Pulse/phase inversion imaging was first reported for both the contrast-enhanced B-mode and the Doppler imaging [75]. It employs two mutually phase-inverted pulses sent by the transducer in quick succession, and the resulting echoes are summed [74]. The signal from tissue shows an identical response to the phase-inverted pulses. The signal from UCA demonstrates a different response to the phase-inverted pulses, allowing the detection of perfused regions. Pulse inversion is available on commercial systems and has been reported extensively [76], [77]. Pulse inversion also has been combined with several other techniques such as coded excitation and ultrafast imaging [16], [78], which are described in later sections. Motion artifacts in pulse inversion can be reduced by applying correction methods [79].

2) SECOND-ORDER ULTRASOUND FIELD (SURF) IMAGING

SURF imaging is another multipulse contrast-enhanced imaging technique. Two ultrasound pulses are transmitted

simultaneously, with their center frequencies differing by 7–10 fold [80]. A low-frequency (0.5–2 MHz) pulse alters the scattering cross-section of the contrast agent. This pulse is chosen based on the resonant frequency of the UCA. A second high-frequency pulse (3–14 MHz) detects the signals generated in response to low-frequency excitation. This approach offers a high spatial resolution, but requires a dual-frequency transducer. Masoy et al. built an annular array for SURF [80] and achieved a CTR of 15–40 dB. Hansen and Angelsen performed SURF imaging using a dual-band linear array with 1.2 MHz and 10 MHz frequency elements [81], achieving a CTR of 8–14 dB. SURF imaging can potentially be used for applications such as breast, thyroid, carotid, and prostate imaging.

3) RADIAL MODULATION

Bouakaz et al. reported microbubble detection based on radial modulation imaging (RMI) [82]. A low-frequency excitation pulse with low amplitude is used to cause microbubble oscillations. A broadband high-frequency imaging pulse pair is then sent to interact with the microbubbles when they are either in the compressed or in the expanded state. Subsequently, the received signals are subtracted. The tissue response to the high-frequency waves does not change due to the low-frequency modulation pulse; thus, the background signal is canceled. However, the differences in the scattering cross-section of the microbubbles when they are compressed vs. expanded results in a residual microbubble response. The performance of high-frequency RMI using a bandlimited IVUS was evaluated in a flow phantom [83]. A CTR improvement of 6.8–15.1 dB was achieved over standard B-mode imaging.

Classical RMI requires the synchronized imaging pulses to interrogate the microbubbles during the compression and expansion states. Moreover, the influence from modulation pulses affects the propagation velocity of imaging pulses [81], causing delay between two echoes from a fixed target, which reduces tissue suppression. A modified radial modulation approach captured UCA oscillations at ultrafast frame rate [84]. The beat frequency between the modulation pulse and the PRF was exploited for CEUS. The modulations (in spectral domain of slow time) produced by this approach were then demodulated to obtain the CEUS frames. This approach circumvented pulse synchronization challenges. Microbubble flow speeds lower than 0.05 mL/min were detected, achieving a CTR of 16 dB in vitro [84]. Sufficient frequency separation is required between modulation and imaging pulses to avoid artifacts [85]. Thus, the frequency selection for the imaging pulse is constrained to higher frequencies, resulting in lower imaging depth. Jing et. al. [86] used a very low frequency modulation pulse (100 kHz) with imaging pulses ($\leq$5 MHz) to overcome this challenge.

4) DIFFERENCE FREQUENCY EXCITATION

Chen et al. reported a strategy that employs two excitation beams with slightly different frequencies [87]. The nonlinear interaction of the two excitation frequencies with microbubbles produces acoustic emissions at the difference frequency and two times the difference frequency. The authors showed that the harmonic signal of the difference frequency signal is generated primarily by resonant microbubbles.

Frinking et al. reported a method that relies on multiple broadband excitation pulses of high frequency along with another burst to destroy UCA [88]. Imaging pulses were used to visualize the region of interest before and after UCA rupture. Contrast agent was detected by either correlating or subtracting the echoes received from imaging pulses, with up to 22 dB enhancement in vitro.

5) AMPLITUDE/POWER MODULATION

Amplitude/Power modulation is a multipulse technique that is commercially available. Two pulses are transmitted such that one pulse is twice in amplitude as the other [89]. The echo received from the low amplitude pulse is scaled by two and subtracted from the echoes obtained using the high amplitude pulse, which cancels the linear tissue response. However, nonlinearity results in a residual contrast-specific signal from UCA perfused regions. Amplitude modulation has also been combined with Doppler imaging [90], subharmonic, harmonic, and coded-excitation imaging [67], [91]. The main limitations of this technique are reduced frame rates and potential motion artifacts. Li et al. employed amplitude modulation and chirp pulses to increase imaging depth without sacrificing resolution [92]. Proprietary multipulse techniques have also been reported, such as cadence contrast pulse sequencing (Siemens), which combines phase and amplitude modulation [93].

6) CHIRP REVERSAL IMAGING

Chirp reversal imaging employs two mutually time-reversed chirps – an ‘‘up-sweep’’ (increasing frequency), and a ‘‘down-sweep’’ (decreasing frequency) chirp. The summation of the resulting signals results in tissue suppression. However, the ring-down effect of the microbubble population is different for an up-sweep relative to the down-sweep chirp. Thus, the microbubble response is retained, enhancing CTR. Like other multipulse techniques, chirp reversal is limited by reduced frame rate, potential motion artifacts, and needs specialized hardware. This method is combined with traditional filtering strategies to avoid motion artifacts [94], [95], [96].

7) SECOND HARMONIC INVERSION

Pasovic et al. proposed second harmonic inversion to reduce the tissue-generated harmonics and enhance the CTR [97]. Two pulses with the same frequency and amplitude were used, but having a phase difference of 90 degrees at the fundamental frequency. They achieved up to 20 dB suppression of tissue harmonics over the axial range of 30–130 mm, albeit at the expense of a reduced frame rate. More research needs to be performed to assess this technique’s performance in vivo and potential artifacts in images.

8) COUNTER-PROPAGATION IMAGING

Multipulse techniques such as PI, AM, and chirp reversal are not entirely specific to microbubbles because of nonlinear propagation. Nonlinear propagation through microbubble suspensions can produce ''pseudo enhancement'' artifacts in distal regions [98]. These artifacts are pronounced even at acoustic pressures lower than 200 kPa. An example is the ''far wall artifact'' while imaging the carotid artery.

Renaud et al. exploited the interaction of two waves propagating in opposite directions for CEUS [98]. The pulses were fired at the transducer bandwidth's low and high-frequency ends. The lower frequency waves were also transmitted without the high-frequency wave as a reference. Counter-propagation imaging exploits that fact that tissues exhibit linear dependence of the elastic modulus on the applied acoustic pressure. Therefore, the counter-propagating pulses are not modified after they pass over each other. However, UCA suspension shows significant nonlinearity even at low pressures, which changes the waves through nonlinear interactions. Comparing the reference signal (when only low-frequency wave is transmitted) to the echoes received when both high and low-frequency pulses are transmitted enables CEUS. The counter-propagation technique did not produce pseudo enhancement in the regions distal to the microbubble cloud [99]. However, this technique is suited only for superficial targets such as carotid or femoral arteries because of physical limitations in producing counter-propagating waves in situ.

9) DESTRUCTION-REPERFUSION

Destruction-Reperfusion imaging uses a combination of high MI and low MI pulses for CEUS. Disrupting the microbubbles with a MI pulse and then imaging with low MI can provide quantitative information of blood flow within a selected region of interest [100]. In this approach, microbubbles are continuously injected such that the influx of microbubbles equals the steady-state clearance. The microbubbles in a single plane are then destroyed, and the refill rate is monitored over time. The refill rate curve obtained is used to extract parameters such as the time to peak intensity, blood flow velocity, blood volume, and mean transit time, which contain valuable diagnostic information [101], [102], [103]. Parametric imaging has also been reported by the bolus transit method [104]. However, microbubble clearance and dosage restrictions limit repeated measurements with this approach [105].

IV. FILTERING/PULSE COMPRESSION APPROACHES

A. MATCHED AND MISMATCHED FILTERING

Matched and mismatched filtering have been used for pulse compression in medical ultrasound imaging [68]. In matched filtering, an a priori estimate of the transmitted signal is correlated with the received echoes. Most CEUS approaches employ nonlinear modes; thus, the filter is matched to the nonlinear frequency band. Pulse compression in matched filtering is proportional to the time-bandwidth product of the filter. Although side lobes are observed, mismatched filtering by tapering the matched filter reduces this artifact [68]. However, this approach causes main-lobe broadening and reduces axial resolution.

B. FRACTIONAL FOURIER TRANSFORM/FAN CHIRP TRANSFORM

Techniques such as Fractional Fourier Transform and Fan Chirp Transform have been investigated to overcome the limitations of pulse compression by matched filtering [106], [107]. The use of short pulses for superharmonic imaging (wideband excitation) enhances axial resolution. However, a significant spectral overlap is observed in the generated harmonics, which makes filtering challenging. Further, this spectral leakage causes range side lobes after pulse compression. These techniques map signals of interest into new domains that facilitate pulse compression. Fractional Fourier Transform analyses signals by rotating the waveforms to a domain between time and frequency [67]. Fan Chirp Transform (FChT) uses a fan-shaped kernel. It reshapes the time-frequency plane into a fan geometry. Accordingly, the FChT compresses a linear chirp along with its harmonics. Therefore, FChT is particularly useful for second harmonic imaging. FChT can achieve over 50 dB range sidelobe suppression in superharmonic imaging with chirps [108].

C. VOLTERRA FILTER

Volterra filter (VF) is a nonlinear series that incorporates memory [109]. It decomposes the input into the sum of linear and other higher-order nonlinear filter components. The total number of filter components determines the order of the VF. Once the filter parameters of the finite order VF are fine-tuned, they can be used to obtain corresponding linear, quadratic, cubic, and other higher order filter responses.

The filter coefficients for second-order VF were obtained by solving a minimum-norm least-squares (MNLS) problem using equations derived from beamformed RF data [109]. The quadratic component of the VF enhanced CTR without sacrificing spatial resolution. Compared to harmonic images, the quadratic VF images retained the low scattering regions of interest due to their vast dynamic range. Du et al. used an adaptive third-order VF to detect UCA [110]. The images acquired using the quadratic and cubic component provided up to 2 to 7 dB higher mean CTR values than B-mode and PI. The VF can extract nonlinear parts of echo data across the entire spectrum, rather than at the fixed bands, resulting in enhanced resolution. Limited work has been reported using this approach; further studies are required in vivo and in clinical conditions.

D. PHASE-LAG IMAGING

Cumulative Phase Delay (CPD) is observed between the fundamental and second harmonic components when ultrasound passes through UCA, but is absent in tissue [111]. Phase lag

was exploited by Demi et al. to improve CTR. The CPD imaging approach outperformed speed of sound-based detection for ultrasound tomography imaging in vivo. CPD imaging offers better temporal resolution than multipulse techniques because it relies on a single transmission. However, bandwidth and UCA size distribution and concentration may affect the phase delay [111], [112].

Under an acoustic pressure of tens of kPa, the transition of phospholipid shell from stiff to buckled state affects UCA scattering. Tremblay-Darveau et al. demonstrated the importance of this mechanism in amplitude modulated contrast pulse sequences [113]. They measured CTR in AM, PI, and AMPI (amplitude modulation pulse inversion) in vitro. Marmottant model simulations showed a negative phase lag in microbubbles undergoing shell softening and a positive phase lag in microbubbles undergoing shell hardening. AM pulses produced 10-15 dB stronger nonlinear signal than PI, for all three microbubble types. At lower insonation pressures (<200 kPa), AM and AMPI provided better CTR than PI. The phase lag caused imperfect cancellation between the half and full amplitude pulse echoes, resulting in a robust nonlinear signal 10–20 dB higher than the second harmonics.

E. TIME REVERSAL ACOUSTICS

The time invariance of the wave equation in a nonlinear regime can be exploited for tissue harmonic cancellation [114]. The time-reversal (TR) technique uses time invariance for perfusion imaging in deeper organs. Couture et al. reported TR combined with PI [115]. These authors used PI with opposite phases correcting for the frequency-dependent phenomenon and then using TR for imaging. Instead of getting the TR signal theoretically [116], they acquired echoes from a copper wire and used them for imaging after time reversal. TR maintained the contrast at high pressures, but injected additional second harmonics at low pressures. The echoes at the onset and end of the pulses remained after applying PI and TR. This approach reduced the tissue harmonic signal by 17.6–32 dB [115].

F. DECORRELATION

In CEUS, the term 'decorrelation' refers to exploiting the loss of correlation in the echo signal from microbubbles and background. Suppressing the echo signal from highly echogenic tissue can be challenging using nonlinear imaging methods alone. Herbst et al. proposed the combination of pulse inversion and acoustic radiation force (ARF) to successfully correlate signals from MBs and tissues. This approach was termed ARF decorrelation-weighted PI (ADW-PI). Pulse inversion images were combined with interframe signal decorrelation data (Figure 3). ARF caused MBs to displace causing echo decorrelation, which was exploited for CTR improvement. Also, the decorrelation data was combined with harmonic filtering methods to obtain enhanced CTR [117]. This approach has also been reported for 3D velocity and flow measurement in blood vessels using CEUS [105].

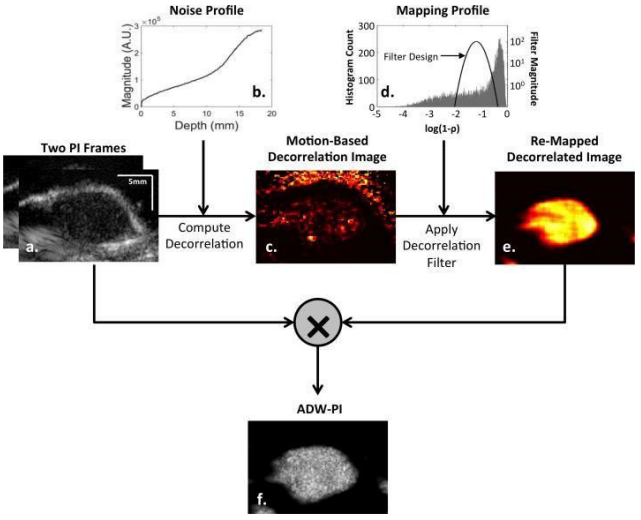

FIGURE 3. Acoustic Radiation Force Decorrelation Weighted PI (ADW-PI) image of mouse tumor. (a) Signal decorrelation between pre and post-ARF PI frames was measured. (b) Decorrelation due to electronic noise was calculated. (c) "Motion-based decorrelation" image was obtained by subtracting (b) from the raw decorrelation image. (d) A Gaussian-shaped remapping filter was used to eliminate low decorrelation tissue signal and high decorrelation noise signal. (e) Decorrelation-weighted remapping filter was used to weight the intensity of either of the original PI frames. (f) The final ADW-PI image. Reprinted from Investigative Radiology, Volume 52 - Issue 2, Herbst et al., "The Use of Acoustic Radiation Force Decorrelation-Weighted Pulse Inversion for Enhanced Ultrasound Contrast Imaging", p 95-102.

G. WAVELETS

A Doinikov model-based bubble wavelet transform technique [118] was reported to boost the contrast from the microbubble region relative to the tissue region. A mother wavelet known as a bubble wavelet was formed, based on simulations of the response of a microbubble to ultrasound. Then, a convolution was performed between the bubble wavelet and the signal processed at various scales. The bubble wavelet transform (BWT) yields a sequence of wavelet coefficients that relate the wavelet and the received signal at a given scale. This approach improved contrast because of the similarity of the frequency range of the bubble wavelet and the UCA signal. Further studies are needed to assess the potential of these techniques in the clinical setting.

H. SPATIOTEMPORAL CLUTTER FILTERING

Tissue signals demonstrate high spatiotemporal coherence unlike UCA signals. Therefore, Singular Value Decomposition (SVD) can differentiate UCA from tissue, especially with ultrafast acquisition [120]. Spatiotemporal filtering was also reported with Non-Local Means (NLM) filtering and accurate monitoring of UCA was achieved with bipartite graph-based tracking [121]. This NLM based spatiotemporal filter helped in retaining the microbubble tracks generated by its movement and reduced background noise. Ito et al. proposed a technique based on spatiotemporal analysis of the pixel

intensity variation over several frames [122]. The variance in intensity differences of consecutively sampled smoothened frames was evaluated for each pixel. Next, masking and thresholding of each variance image frame was performed with respect to a binarized image frame obtained using the discriminant analysis method. The feasibility of visualizing blood vessels in the mouse tail was demonstrated using the proposed approach [122].

I. EMPIRICAL MODE DECOMPOSITION

Empirical Mode Decomposition (EMD) can be used to differentiate nonlinear signals from UCA and tissue [123]. EMD is a fundamental part of the Hilbert-Huang transform (HHT). HHT is suitable for analyzing nonlinear and non-stationary signals and involves two steps: EMD and Hilbert analysis. EMD decomposes the data into several Intrinsic Mode Functions (IMFs). IMF is a term given to the signal's oscillatory mode that represents the signal's highest local frequency. To extract the oscillatory mode, EMD begins by defining local maxima and minima of all signals, which form upper and lower envelopes. The average of the two envelopes is measured and subtracted from the original signal. This subtracted part is the IMF function, and the residue obtained is used to repeat the process, known as sifting. The process is considered complete when the difference in standard deviation between the consecutive observations of the IMF function or the residue falls below a fixed threshold, or when no further IMFs can be produced. Most noise energy gets decomposed into IMFs, leading to a significant improvement in image contrast.

Liao et al. demonstrated the effectiveness of EMD in second-harmonic imaging to improve CTR. Extensions of EMD, called Ensemble Empirical Mode Decomposition (EEMD) and Bi-dimensional Empirical Mode Decomposition (BEMD), were also reported to enhance CTR [124].

V. ULTRAFAST IMAGING APPROACHES

A variety of ultrafast imaging approaches have been reported. A proprietary ultrafast CEUS technique is also commercially available in SuperSonic™MACH™systems (Hologic Supersonic Imagine).

A. ULTRAFAST CEUS DOPPLER

Ultrafast Doppler imaging has been combined with CEUS, for assessment of flow and vessel mapping [125], [126]. Bruce et al. used a plane-wave acquisition approach combined with nonlinear Doppler processing at 15 MHz [127]. This approach increased microvascular blood flow resolution while compensating for the weaker high-frequency microbubble response. An amplitude-modulated sequence was generated for each angle of a multi-angle plane-wave sequence, resulting in a nonlinear-Doppler pulse, which was repeated to create a nonlinear sequence. The pulsing sequences were summed to create a nonlinear image for each angle, which were then compounded. Desailly et al. used SVD processing on linear ultrafast ultrasound images for

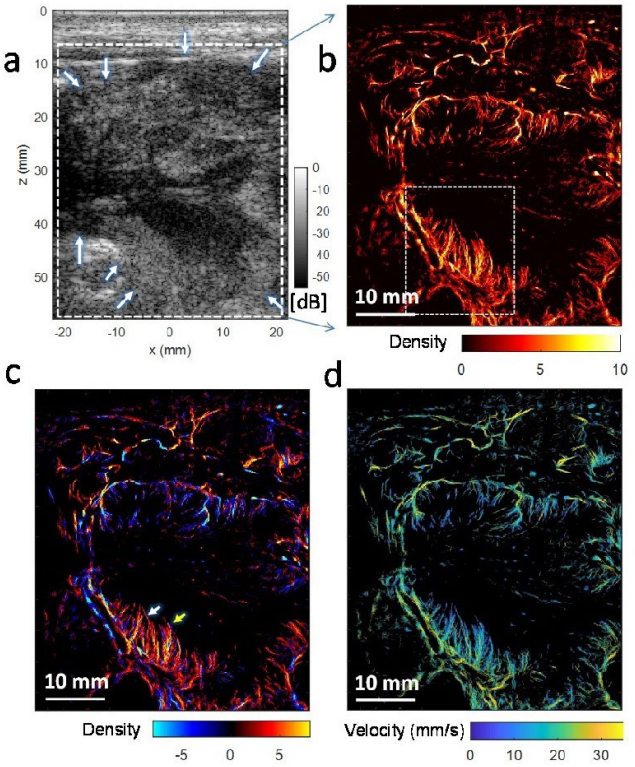

FIGURE 4. In-vivo Super-resolution Imaging (a) B-mode image of human pancreatic tumor, (white arrows show approximate lesion boundary) (b) Super-resolution microvessel intensity image (c) Corresponding bi-directional microvessel intensity image (red and blue colors indicate upward and downward flow, respectively) (d) Super-resolution microvessel velocity image (colormap shows the magnitude). Reprinted from Physics in Medicine & Biology, Volume 66, Number 8, Chengwu Huang et al. 2021, "Super-resolution ultrasound localization microscopy based on a high frame-rate clinical ultrasound scanner: an in-human feasibility study", Physics in Medicine & Biology, DOI:https://doi.org/10.1088/1361-6560/abef45 © Institute of Physics and Engineering in Medicine. Reproduced by permission of IOP Publishing. All rights reserved.

CEUS Doppler [126]. For each dataset, the singular value thresholds were determined, and they distinguished singular vectors with high spatiotemporal coherence from those with lower coherence. Subsequently, the consecutive frames were summed as for nonlinear Doppler data after being filtered by SVD.

Traditional contrast techniques (e.g., PI) and Doppler with long ensembles can be combined at high frame rates to enhance microbubble detection [78], [128]. Long Doppler ensembles can be used with contrast agent-specific techniques without significantly affecting microbubble scattering coherence at low MI. Repeated insonation can change the acoustic response from microbubbles over time, degrading the Doppler signal and decorrelating the echoes. Using low insonation pressures can reduce this effect. Quantitative Doppler imaging has also been combined with amplitude modulation to visualize microvasculature with up to 17 dB higher CTR than PI-Doppler [90].

B. ULTRASOUND SUPER RESOLUTION (USR) IMAGING

Several in vitro, animal [129], [130], [131], and human studies [132], [133]) have been reported on USR. A prominent super-resolution CEUS approach relies on locating the centroid of individual microbubble Point Spread Function (PSF) to localize the microbubble [134], [135], [136]. Accumulating localizations captured through several planes by ultrafast imaging produces a super-resolved image ($\sim$10 μm resolution) of the microvasculature and flow velocity maps [129], [131], [135].

Previous reports focus on super-resolution imaging in organs such as kidney [137], breast [137], and lower limb [132]. Huang et al. demonstrated super-resolution to image pancreatic tumors in humans (Figure 4). Larger-sized contrast agent populations (3–4 μm and 5–8 μm) improved the performance of super-resolution versus 1–2 μm microbubbles [138]. Research is also being directed towards achieving 3D super-resolution [139], [140]. Nonlinear contrast pulse sequencing has also been used for super-resolution ultrasound imaging [141]. Furthermore, studies are being conducted to overcome the limitations of long acquisition time [130], [142] motion artifacts, accuracy [143], and the limit on the concentration of microbubbles [144].

A Super-resolution Optical Fluctuation Imaging [142] (SOFI)-inspired approach exploits the movement of microbubbles along the vessels to induce correlated fluctuation in adjacent pixels along the streamlines and uncorrelated variations in different vessels. Consequently, SOFI enables the differentiation of adjacent blood vessels and a smooth depiction of the blood vessels along the streamlines. AI-based approaches inspired by optical microscopy have also been reported [145]. Deep learning (DL) may be used in ULM imaging to boost imaging efficiency and implementation flexibility [147]. By using the sub-pixel convolution layer, the computational and memory complexity can be reduced. The image resolution can also be improved by using normal up-sampling and transposed convolutions, which are implemented using an encoder-decoder network, similar to the U-Net architecture [146]. Liu et al. used a modified sub-pixel convolutional neural network in ULM (mSPCN-ULM), which increased data processing speed and accuracy [147]. DL is also useful in the spatiotemporal filtering of USR images. A three-dimensional convolutional neural network (3DCNN) was reported to reduce clutter significantly [148]. The main challenges of super-resolution imaging with respect to clinical translation are acquisition times and high data volumes. The reader is directed to [14] and [136] for a more exhaustive review of USR.

VI. FUTURE PERSPECTIVES

Physical insights from modeling and laboratory experiments on UCA have led to new CEUS imaging approaches. Many of the reported approaches have shown technical feasibility, but have not been evaluated in vivo and in human trials. Adequate funding and investment is needed for continued development of this technology in animals and clinical systems. The global CEUS market is currently USD 1.8 billion in 2020 and is expected to grow at a compound annual growth rate of 4.0% from 2021 to 2028 [138]. The USA has the largest ultrasound market, but only a limited number of FDA-approved applications exist for CEUS, which has reduced growth. Off-label use is prevalent but not typically covered for reimbursement [150].

Another challenge is the lack of data on many techniques in conditions representative of clinical imaging. In most studies, work is reported using homogeneous tissue-mimicking phantoms. The attenuation coefficient of the phantom and the depth of the target may not model realistic clinical conditions. Even studies on small animals typically consider an ''optimistic scenario'' because of the tumors' superficial depth, unlike clinical tumors that are usually seated several centimeters deep. Further, the heterogeneity of tissue can degrade images because of attenuation, phase aberration, and reverberation clutter [26].

Deeper tissue necessitates the use of lower frequencies, which reduces imaging resolution. The lower excitation pressures used in non-disruptive techniques reduces SNR [151]. Coded pulsing, pulse compression, and beamforming techniques that are specific to CEUS can be investigated further to address this challenge. Synthetic transmit focusing techniques could be employed to reduce MB disruption, albeit at the cost of potential motion artifacts [152], [153]. Hardware and computational enhancements can enable real-time implementation of methods that were previously considered impractical. For example, we may expect improved transducer bandwidths using CMUT transducer arrays, and real-time 3D CEUS using graphics processing unit (GPU) computing. Lower-end systems and specialized applications, such as IVUS imaging, may continue to rely on techniques that require simple hardware and processing.

Most contrast-specific techniques either need arbitrary waveform generation or perform better with this capability. The excitation circuitry of commercial ultrasound systems rely on either square wave pulsers or linear amplifiers [154]. Linear amplifiers can output arbitrary waveforms without introducing harmonic distortion and are thus advantageous for CEUS [155], [156], [157]. However, most commercial systems use square wave pulsers because they are simple, inexpensive, compact, and power efficient [154], [158]. Advances in microelectronics may make it cost-effective to incorporate pulse amplifiers, enabling a wider range of approaches to be translated.

In the next decade, techniques based on plane wave (ultrafast) imaging may become more widely available on clinical scanners. Applications of super-resolution imaging are still emerging that could enable insights into disease mechanisms, progression, and therapeutic assessment. The narrow field of view of super-resolution imaging may be addressed through advancement in 3D imaging. Theoretical considerations suggest up to ten-fold improvement in resolution over the ultrasonic diffraction limit, however only up to five-fold enhancement is typically achieved.

Advances in microbubble detection, isolation and motion correction algorithms can help improve resolution further. Detection and localization of individual bubbles in microvessels using nonlinear imaging approaches may be an important area of investigation. Further, approaches such as sparse signal processing and beamforming could be used to reduce computational overhead. Application of machine learning in super-resolution imaging will likely grow rapidly in the near future [159], [160]. Data complexity reduction, and employing higher contrast agent concentration will help translate super-resolution imaging to the clinic. Competing approaches such as photoacoustics imaging also exist for imaging vasculature. More research is necessary to establish clinical indications for super-resolution imaging.

In the near future, monodisperse contrast agents and contrast agents designed for specific imaging modes may become available clinically. Approaches for quantitative estimation and system independent assessment of contrast agent perfusion will also be a likely area of advancement. Improvement in the understanding of complex contrast agent behavior such as bubble-bubble interaction and multiple scattering may help improve quantitation of CEUS parameters.

The performance of CEUS also depends on the type of probe used. User-defined settings, such as dynamic range and gain, also affect performance, and thus, techniques for automatic setting of these parameters may be an area of research inquiry. Consensus would be needed over choice of optimal imaging parameters, contrast agent dose, and preferred clinical indications for techniques on the horizon.

Despite the aforementioned challenges, the field of CEUS continues to grow. Previously, many of the reported techniques were considered to be only of academic interest. However, some of these techniques may now find niche applications. Therefore, more preclinical and clinical research is required to translate promising approaches to the clinic. In the next decade, one can expect new technologies becoming available commercially/clinically and enabling the wider application of CEUS in preclinical models, as well as for in vivo diagnosis and treatment monitoring/longitudinal assessment of therapy.

ACKNOWLEDGMENT

The authors would like to thank Prof. Karla P. Mercado-Shekhar and Pratibha for their helpful suggestions.

REFERENCES

[1] M. A. Averkiou, M. F. Bruce, J. E. Powers, P. S. Sheeran, and P. N. Burns, "Imaging methods for ultrasound contrast agents," *Ultrasound Med. Biol.*, vol. 46, no. 3, pp. 498–517, Mar. 2020.

[2] N. Laugesen, C. Nolsoe, and J. Rosenberg, "Clinical applications of contrast-enhanced ultrasound in the pediatric work-up of focal liver lesions and blunt abdominal trauma: A systematic review," *Ultrasound Int. Open*, vol. 3, no. 1, pp. E2–E7, Feb. 2017.

[3] P. Frinking, T. Segers, Y. Luan, and F. Tranquart, "Three decades of ultrasound contrast agents: A review of the past, present and future improvements," *Ultrasound Med. Biol.*, vol. 46, no. 4, pp. 892–908, Apr. 2020.

[4] K. S. Mehta, J. J. Lee, A. A. Taha, E. Avgerinos, and R. A. Chaer, "Vascular applications of contrast-enhanced ultrasound imaging," *J. Vascular Surg.*, vol. 66, no. 1, pp. 266–274, Jul. 2017.

[5] E. H. Chang, "An introduction to contrast-enhanced ultrasound for nephrologists," *Nephron*, vol. 138, no. 3, pp. 176–185, 2018.

[6] A. Ignee, N. S. S. Atkinson, G. Schuessler, and C. F. Dietrich, "Ultrasound contrast agents," *Endosc. Ultrasound*, vol. 5, no. 6, p. 355, Nov. 2016.

[7] V. Paefgen, D. Doleschel, and F. Kiessling, "Evolution of contrast agents for ultrasound imaging and ultrasound-mediated drug delivery," *Frontiers Pharmacol.*, vol. 6, p. 197, Sep. 2015.

[8] C. M. Moran, "Ultrasonic contrast agents," *Clin. Ultrasound*, vol. 1, pp. 77–89, Apr. 2011.

[9] A. Ding, N. Kulkarni, F. J. Fintelmann, and S. Saini, "Liver: Normal anatomy and examination techniques," in *Textbook of Gastrointestinal Radiology, 2-Volume Set*, 4th ed., R. M. Gore and M. S. Levine, Eds. Philadelphia, PA, USA: Saunders, 2015, ch. 83, pp. 1471–1497. [Online]. Available: https://www.sciencedirect.com/science/article/pii/B9781455751174000830, doi: 10.1016/B978-1-4557-5117-4.00083-0.

[10] E. Quaia, *Classification and Safety of Microbubble-Based Contrast Agents*. Berlin, Germany: Springer, 2005.

[11] N. de Jong, P. J. A. Frinking, A. Bouakaz, and F. J. T. Cate, "Detection procedures of ultrasound contrast agents," *Ultrasonics*, vol. 38, nos. 1–8, pp. 87–92, Mar. 2000.

[12] P. J. A. Frinking, A. Bouakaz, J. Kirkhorn, F. J. Ten Cate, and N. de Jong, "Ultrasound contrast imaging: Current and new potential methods," *Ultrasound Med. Biol.*, vol. 26, no. 6, pp. 965–975, Jul. 2000.

[13] P. Phillips and E. Gardner, "Contrast-agent detection and quantification," *Eur. Radiol.*, vol. 14, no. 8, pp. 4–10, Oct. 2004.

[14] O. Couture, V. Hingot, B. Heiles, P. Muleki-Seya, and M. Tanter, "Ultrasound localization microscopy and super-resolution: A state of the art," *IEEE Trans. Ultrason., Ferroelectr., Freq. Control*, vol. 65, no. 8, pp. 1304–1320, Aug. 2018.

[15] N. de Jong, A. Bouakaz, and F. J. Ten Cate, "Contrast harmonic imaging," *Ultrasonics*, vol. 40, no. 1, pp. 567–573, Dec. 2002.

[16] D. H. Simpson, C. Ting Chin, and P. N. Burns, "Pulse inversion Doppler: A new method for detecting nonlinear echoes from microbubble contrast agents," *IEEE Trans. Ultrason., Ferroelectr., Freq. Control*, vol. 46, no. 2, pp. 372–382, Mar. 1999.

[17] D. E. Goertz et al., "High frequency nonlinear B-scan imaging of microbubble contrast agents," *IEEE Trans. Ultrason., Ferroelectr., Freq. Control*, vol. 52, no. 1, pp. 65–79, Jan. 2005.

[18] M.-X. Tang, N. Kamiyama, and R. J. Eckersley, "Effects of nonlinear propagation in ultrasound contrast agent imaging," *Ultrasound Med. Biol.*, vol. 36, no. 3, pp. 459–466, Mar. 2010.

[19] D. E. Goertz, M. E. Frijlink, N. de Jong, and A. F. W. van der Steen, "Nonlinear intravascular ultrasound contrast imaging," *Ultrasound Med. Biol.*, vol. 32, no. 4, pp. 491–502, Apr. 2006.

[20] H. Shekhar, J. J. Rychak, and M. M. Doyley, "Modifying the size distribution of microbubble contrast agents for high-frequency subharmonic imaging," *Med. Phys.*, vol. 40, no. 8, Jul. 2013, Art. no. 082903.

[21] H. Shekhar and M. M. Doyley, "Improving the sensitivity of high-frequency subharmonic imaging with coded excitation: A feasibility study," *Med. Phys.*, vol. 39, no. 4, pp. 2049–2060, Mar. 2012.

[22] E. Biagi, L. Breschi, E. Vannacci, and L. Masotti, "Subharmonic emissions from microbubbles: Effect of the driving pulse shape," *IEEE Trans. Ultrason., Ferroelectr., Freq. Control*, vol. 53, no. 11, pp. 2174–2182, Nov. 2006.

[23] L. Masotti, E. Biagi, L. Breschi, and E. Vannacci, "Study and characterization of subharmonic emissions by using shaped ultrasonic driving pulse," in *Acoustical Imaging* (Acoustical Imaging), vol. 28. Dordrecht, The Netherlands: Springer, 2007, doi: 10.1007/1-4020-5721-0_33.

[24] V. Daeichin, T. Faez, G. Renaud, J. G. Bosch, A. F. W. van der Steen, and N. de Jong, "Effect of self-demodulation on the subharmonic response of contrast agent microbubbles," *Phys. Med. Biol.*, vol. 57, no. 12, pp. 3675–3691, Jun. 2012.

[25] J. Sijl et al., "Subharmonic behavior of phospholipid-coated ultrasound contrast agent microbubbles," *J. Acoust. Soc. Amer.*, vol. 128, no. 5, pp. 3239–3252, Nov. 2010.

[26] D. Zhang, Y. Gong, X. Gong, Z. Liu, K. Tan, and H. Zheng, "Enhancement of subharmonic emission from encapsulated microbubbles by using a chirp excitation technique," *Phys. Med. Biol.*, vol. 52, no. 18, pp. 5531–5544, Sep. 2007.

[27] H. Shekhar and M. M. Doyley, "The response of phospholipid-encapsulated microbubbles to chirp-coded excitation: Implications for high-frequency nonlinear imaging," *J. Acoust. Soc. Amer.*, vol. 133, no. 5, pp. 3145–3158, May 2013.

[28] D. Zhang, X. Xi, Z. Zhang, X. Gong, G. Chen, and J. Wu, "A dual-frequency excitation technique for enhancing the sub-harmonic emission from encapsulated microbubbles," *Phys. Med. Biol.*, vol. 54, no. 13, pp. 4257–4272, Jul. 2009.

[29] E. Kanbar, D. Fouan, C. A. Sennoga, A. A. Doinikov, and A. Bouakaz, "Impact of filling gas on subharmonic emissions of phospholipid ultrasound contrast agents," *Ultrasound Med. Biol.*, vol. 43, no. 5, pp. 1004–1015, May 2017.

[30] H. Shekhar, I. Awuor, K. Thomas, J. J. Rychak, and M. M. Doyley, "The delayed onset of subharmonic and ultraharmonic emissions from a phospholipid-shelled microbubble contrast agent," *Ultrasound Med. Biol.*, vol. 40, no. 4, pp. 727–738, Apr. 2014.

[31] A. Katiyar and K. Sarkar, "Excitation threshold for subharmonic generation from contrast microbubbles," *J. Acoust. Soc. Amer.*, vol. 130, no. 5, pp. 3137–3147, Nov. 2011.

[32] V. Daeichin, J. G. Bosch, A. Needles, F. S. Foster, A. van der Steen, and N. de Jong, "Subharmonic, non-linear fundamental and ultraharmonic imaging of microbubble contrast at high frequencies," *Ultrasound Med. Biol.*, vol. 41, no. 2, pp. 486–497, Feb. 2015.

[33] D. Maresca et al., "Contrast-enhanced intravascular ultrasound pulse sequences for bandwidth-limited transducers," *Ultrasound Med. Biol.*, vol. 39, no. 4, pp. 706–713, Apr. 2013.

[34] H. Shekhar, J. S. Rowan, and M. M. Doyley, "Combining subharmonic and ultraharmonic modes for intravascular ultrasound imaging: A preliminary evaluation," *Ultrasound Med. Biol.*, vol. 43, no. 11, pp. 2725–2732, Nov. 2017.

[35] D. E. Goertz et al., "Subharmonic contrast intravascular ultrasound for vasa vasorum imaging," *Ultrasound Med. Biol.*, vol. 33, no. 12, pp. 1859–1872, Dec. 2007.

[36] A. Sridharan et al., "Characterizing breast lesions using quantitative parametric 3D subharmonic imaging: A multicenter study," *Academic Radiol.*, vol. 27, no. 8, pp. 1065–1074, Aug. 2020.

[37] F. Forsberg et al., "In vivo perfusion estimation using subharmonic contrast microbubble signals," *J. Ultrasound Med.*, vol. 25, no. 1, pp. 15–21, Jan. 2006.

[38] F. Forsberg et al., "3D harmonic and subharmonic imaging for characterizing breast lesions: A multi-center clinical trial," *J. Ultrasound Med.*, vol. 41, no. 7, pp. 1667–1675, Jul. 2022.

[39] P. Machado et al., "Hepatic vein contrast-enhanced ultrasound subharmonic imaging signal as a screening test for portal hypertension," *Digestive Diseases Sci.*, vol. 66, no. 12, pp. 4354–4360, Dec. 2021.

[40] H. Lu et al., "Correlation between portal vein pressure and subharmonic scattering signals from SonoVue microbubbles in canines," *Ultrasound Med. Biol.*, vol. 49, no. 1, pp. 203–211, Jan. 2023.

[41] X. Qiao, Y. Wen, J. Yu, A. Bouakaz, Y. Zong, and M. Wan, "Non-invasive pressure estimation based on the subharmonic response of SonoVue: Application to intracranial blood pressure assessment," *IEEE Trans. Ultrason., Ferroelectr., Freq. Control*, vol. 69, no. 3, pp. 957–966, Mar. 2022.

[42] A. Q. X. Nio et al., "Optimal control of SonoVue microbubbles to estimate hydrostatic pressure," *IEEE Trans. Ultrason., Ferroelectr., Freq. Control*, vol. 67, no. 3, pp. 557–567, Mar. 2020.

[43] A. Bouakaz, S. Frigstad, F. J. Ten Cate, and N. de Jong, "Improved contrast to tissue ratio at higher harmonics," *Ultrasonics*, vol. 40, nos. 1–8, pp. 575–578, May 2002.

[44] A. Bouakaz, S. Frigstad, F. J. Ten Cate, and N. de Jong, "Super harmonic imaging: A new imaging technique for improved contrast detection," *Ultrasound Med. Biol.*, vol. 28, no. 1, pp. 59–68, Jan. 2002.

[45] A. Bouakaz, B. J. Krenning, W. B. Vletter, F. J. T. Cate, and N. De Jong, "Contrast superharmonic imaging: A feasibility study," *Ultrasound Med. Biol.*, vol. 29, no. 4, pp. 547–553, Apr. 2003.

[46] K. Martin et al., "Dual-frequency piezoelectric transducers for contrast enhanced ultrasound imaging," *Sensors*, vol. 14, no. 11, pp. 20825–20842, Nov. 2014.

[47] L. Wu, X. Chen, G. Wang, and Q. Zhou, "Dual-frequency piezoelectric micromachined ultrasonic transducers," *Appl. Phys. Lett.*, vol. 115, no. 2, Jul. 2019, Art. no. 023501.

[48] P. L. M. J. van Neer, M. G. Danilouchkine, G. M. Matte, A. F. W. van der Steen, and N. de Jong, "Dual-pulse frequency compounded superharmonic imaging," *IEEE Trans. Ultrason., Ferroelectr., Freq. Control*, vol. 58, no. 11, pp. 2316–2324, Nov. 2011.

[49] M. G. Danilouchkine et al., "Single pulse frequency compounding protocol for superharmonic imaging," *Phys. Med. Biol.*, vol. 58, no. 14, pp. 4791–4805, Jul. 2013.

[50] B. Lindsey, J. Rojas, K. Martin, S. Shelton, and P. Dayton, "Acoustic characterization of contrast-to-tissue ratio and axial resolution for dual-frequency contrast-specific acoustic angiography imaging," *IEEE Trans. Ultrason., Ferroelectr., Freq. Control*, vol. 61, no. 10, pp. 1668–1687, Oct. 2014.

[51] I. G. Newsome and P. A. Dayton, "Visualization of microvascular angiogenesis using dual-frequency contrast-enhanced acoustic angiography: A review," *Ultrasound Med. Biol.*, vol. 46, no. 10, pp. 2625–2635, Oct. 2020.

[52] B. D. Lindsey, S. E. Shelton, and P. A. Dayton, "Optimization of contrast-to-tissue ratio through pulse windowing in dual-frequency 'acoustic angiography' imaging," *Ultrasound Med. Biol.*, vol. 41, no. 7, pp. 1884–1895, Jul. 2015.

[53] A. Guiroy et al., "Dual-frequency transducer for nonlinear contrast agent imaging," *IEEE Trans. Ultrason., Ferroelectr., Freq. Control*, vol. 60, no. 12, pp. 2634–2644, Dec. 2013.

[54] B. D. Lindsey, J. D. Rojas, and P. A. Dayton, "On the relationship between microbubble fragmentation, deflation and broadband superharmonic signal production," *Ultrasound Med. Biol.*, vol. 41, no. 6, pp. 1711–1725, Jun. 2015.

[55] R. C. Gessner, S. R. Aylward, and P. A. Dayton, "Mapping microvasculature with acoustic angiography yields quantifiable differences between healthy and tumor-bearing tissue volumes in a rodent model," *Radiology*, vol. 264, no. 3, pp. 733–740, Sep. 2012.

[56] S. E. Shelton, B. D. Lindsey, P. A. Dayton, and Y. Z. Lee, "First-in-human study of acoustic angiography in the breast and peripheral vasculature," *Ultrasound Med. Biol.*, vol. 43, no. 12, pp. 2939–2946, Dec. 2017.

[57] M. P. J. Kuenen, M. Mischi, and H. Wijkstra, "Contrast-ultrasound diffusion imaging for localization of prostate cancer," *IEEE Trans. Med. Imag.*, vol. 30, no. 8, pp. 1493–1502, Aug. 2011.

[58] S. G. Schalk et al., "4-D spatiotemporal analysis of ultrasound contrast agent dispersion for prostate cancer localization: A feasibility study," *IEEE Trans. Ultrason., Ferroelectr., Freq. Control*, vol. 62, no. 5, pp. 839–851, May 2015.

[59] M. P. J. Kuenen, T. A. Saidov, H. Wijkstra, J. M. C. H. de La Rosette, and M. Mischi, "Correspondence–spatiotemporal correlation of ultrasound contrast agent dilution curves for angiogenesis localization by dispersion imaging," *IEEE Trans. Ultrason., Ferroelectr., Freq. Control*, vol. 60, no. 12, pp. 2665–2669, Dec. 2013.

[60] M. Mischi, M. P. J. Kuenen, and H. Wijkstra, "Angiogenesis imaging by spatiotemporal analysis of ultrasound contrast agent dispersion kinetics," *IEEE Trans. Ultrason., Ferroelectr., Freq. Control*, vol. 59, no. 4, pp. 621–629, Apr. 2012.

[61] S. G. Schalk et al., "Contrast-enhanced ultrasound angiogenesis imaging by mutual information analysis for prostate cancer localization," *IEEE Trans. Biomed. Eng.*, vol. 64, no. 3, pp. 661–670, Mar. 2017.

[62] R. J. van Sloun, L. Demi, A. W. Postema, J. J. de la Rosette, H. Wijkstra, and M. Mischi, "Ultrasound-contrast-agent dispersion and velocity imaging for prostate cancer localization," *Med. Image Anal.*, vol. 35, pp. 610–619, Jan. 2017.

[63] C. F. Dietrich et al., "How to perform contrast-enhanced ultrasound (CEUS)," *Ultrasound Int. Open*, vol. 4, no. 1, p. E2, 2018.

[64] C.-K. Yeh and S.-Y. Su, "Effects of acoustic insonation parameters on ultrasound contrast agent destruction," *Ultrasound Med. Biol.*, vol. 34, no. 8, pp. 1281–1291, Aug. 2008.

[65] J. Borsboom, C. Ting Chin, and N. de Jong, "Experimental evaluation of a non-linear coded excitation method for contrast imaging," *Ultrasonics*, vol. 42, nos. 1–9, pp. 671–675, Apr. 2004.

[66] J. M. G. Borsboom, C. Ting Chin, A. Bouakaz, M. Versluis, and N. de Jong, "Harmonic chirp imaging method for ultrasound contrast agent," *IEEE Trans. Ultrason., Ferroelectr., Freq. Control*, vol. 52, no. 2, pp. 241–249, Feb. 2005.

[67] S. Harput, M. Arif, J. Mclaughlan, D. J. Cowell, and S. Freear, "The effect of amplitude modulation on subharmonic imaging with chirp excitation," *IEEE Trans. Ultrason., Ferroelectr., Freq. Control*, vol. 60, no. 12, pp. 2532–2544, Dec. 2013.

[68] T. Misaridis and J. A. Jensen, "Use of modulated excitation signals in medical ultrasound. Part I: Basic concepts and expected benefits," *IEEE Trans. Ultrason., Ferroelectr., Freq. Control*, vol. 52, no. 2, pp. 177–191, Feb. 2005.

[69] R. J. Eckersley, M.-X. Tang, K. Chetty, and J. V. Hajnal, "Microbubble contrast agent detection using binary coded pulses," *Ultrasound Med. Biol.*, vol. 33, no. 11, pp. 1787–1795, Nov. 2007.

[70] C. Leavens, R. Williams, F. Foster, P. Burns, and M. Sherar, "Golay pulse encoding for microbubble contrast imaging in ultrasound," *IEEE Trans. Ultrason., Ferroelectr., Freq. Control*, vol. 54, no. 10, pp. 2082–2090, Oct. 2007.

[71] C.-C. Shen and T.-Y. Shi, "Golay-encoded excitation for dual-frequency harmonic detection of ultrasonic contrast agents," *IEEE Trans. Ultrason., Ferroelectr., Freq. Control*, vol. 58, no. 2, pp. 349–356, Feb. 2011.

[72] P. Gong, P. Song, and S. Chen, "Hadamard-encoded multipulses for contrast-enhanced ultrasound imaging," *IEEE Trans. Ultrason., Ferroelectr., Freq. Control*, vol. 64, no. 11, pp. 1674–1683, Nov. 2017.

[73] P. Gong, P. Song, C. Huang, and S. Chen, "On combination of Hadamard-encoded multipulses and multiplane wave transmission in contrast-enhanced ultrasound imaging," *IEEE Trans. Ultrason., Ferroelectr., Freq. Control*, vol. 65, no. 10, pp. 1977–1980, Oct. 2018.

[74] C. Shen and J. Yan, "High-order Hadamard-encoded transmission for tissue background suppression in ultrasound contrast imaging: Memory effect and decoding schemes," *IEEE Trans. Ultrason., Ferroelectr., Freq. Control*, vol. 66, no. 1, pp. 26–37, Jan. 2019.

[75] M. Crocco, M. Palmese, C. Sciallero, and A. Trucco, "A comparative analysis of multi-pulse techniques in contrast-enhanced ultrasound medical imaging," *Ultrasonics*, vol. 49, no. 1, pp. 120–125, Jan. 2009.

[76] P. N. Burns, S. R. Wilson, and D. H. Simpson, "Pulse inversion imaging of liver blood flow: Improved method for characterizing focal masses with microbubble contrast," *Invest. Radiol.*, vol. 35, no. 1, pp. 58–71, 2000.

[77] M. Bertolotto, L. D. Palma, E. Quaia, and M. Locatelli, "Characterization of unifocal liver lesions with pulse inversion harmonic imaging after Levovist injection: Preliminary results," *Eur. Radiol.*, vol. 10, no. 9, pp. 1369–1376, Aug. 2000.

[78] M. Toulemonde et al., "High-frame-rate contrast echocardiography using diverging waves: Initial *in vitro* and *in vivo* evaluation," *IEEE Trans. Ultrason., Ferroelectr., Freq. Control*, vol. 65, no. 12, pp. 2212–2221, Dec. 2018.

[79] A. Stanziola et al., "Motion artifacts and correction in multipulse high-frame rate contrast-enhanced ultrasound," *IEEE Trans. Ultrason., Ferroelectr., Freq. Control*, vol. 66, no. 2, pp. 417–420, Feb. 2019.

[80] S.-E. Masoy, O. Standal, P. Nasholm, T. F. Johansen, B. Angelsen, and R. Hansen, "SURF imaging: In vivo demonstration of an ultrasound contrast agent detection technique," *IEEE Trans. Ultrason., Ferroelectr., Freq. Control*, vol. 55, no. 5, pp. 1112–1121, May 2008.

[81] R. Hansen and B. A. J. Angelsen, "SURF imaging for contrast agent detection," *IEEE Trans. Ultrason., Ferroelectr., Freq. Control*, vol. 56, no. 2, pp. 280–290, Feb. 2009.

[82] A. Bouakaz, M. Versluis, J. Borsboom, and N. De Jong, "Radial modulation of microbubbles for ultrasound contrast imaging," *IEEE Trans. Ultrason., Ferroelectr., Freq. Control*, vol. 54, no. 11, pp. 2283–2290, Nov. 2007.

[83] F. T. H. Yu, F. S. Villanueva, and X. Chen, "Radial modulation contrast imaging using a 20-MHz single-element intravascular ultrasound catheter," *IEEE Trans. Ultrason., Ferroelectr., Freq. Control*, vol. 61, no. 5, pp. 779–791, May 2014.

[84] P. Muleki-Seya, K. Xu, M. Tanter, and O. Couture, "Ultrafast radial modulation imaging," *IEEE Trans. Ultrason., Ferroelectr., Freq. Control*, vol. 67, no. 3, pp. 598–611, Mar. 2020.

[85] E. Chérin et al., "Radial modulation imaging of microbubble contrast agents at high frequency," *Ultrasound Med. Biol.*, vol. 34, no. 6, pp. 949–962, Jun. 2008.

[86] B. Jing and B. D. Lindsey, "Very low frequency radial modulation for deep penetration contrast-enhanced ultrasound imaging," *Ultrasound Med. Biol.*, vol. 48, no. 3, pp. 530–545, Mar. 2022.

[87] S. Chen, R. Kinnick, J. F. Greenleaf, and M. Fatemi, "Difference frequency and its harmonic emitted by microbubbles under dual frequency excitation," *Ultrasonics*, vol. 44, pp. 123–126, Jan. 2006.

[88] P. J. A. Frinking, E. I. Cespedes, J. Kirkhorn, H. G. Torp, and N. de Jong, "A new ultrasound contrast imaging approach based on the combination of multiple imaging pulses and a separate release burst," *IEEE Trans. Ultrason., Ferroelectr., Freq. Control*, vol. 48, no. 3, pp. 643–651, May 2001.

[89] G. A. Brock-Fisher, "Means for increasing sensitivity in non-linear ultrasound imaging systems," *J. Acoust. Soc. Amer.*, vol. 101, no. 6, p. 3240, Jun. 1997.

[90] C. Tremblay-Darveau, R. Williams, L. Milot, M. Bruce, and P. N. Burns, "Visualizing the tumor microvasculature with a nonlinear plane-wave Doppler imaging scheme based on amplitude modulation," *IEEE Trans. Med. Imag.*, vol. 35, no. 2, pp. 699–709, Feb. 2016.

[91] R. J. Eckersley, C. T. Chin, and P. N. Burns, "Optimising phase and amplitude modulation schemes for imaging microbubble contrast agents at low acoustic power," *Ultrasound Med. Biol.*, vol. 31, no. 2, pp. 213–219, Feb. 2005.

[92] M.-L. Li, Y.-C. Kuo, and C.-K. Yeh, "Amplitude-modulation chirp imaging for contrast detection," *Ultrasound Med. Biol.*, vol. 36, no. 9, pp. 1535–1545, Sep. 2010.

[93] S. M. Stieger et al., "Imaging of angiogenesis using Cadence^{TM} contrast pulse sequencing and targeted contrast agents," *Contrast Media Mol. Imag.*, vol. 3, no. 1, pp. 9–18, Jan. 2008.

[94] Y. Sun, S. Zhao, P. A. Dayton, and K. W. Ferrara, "Observation of contrast agent response to chirp insonation with a simultaneous optical-acoustical system," *IEEE Trans. Ultrason., Ferroelectr., Freq. Control*, vol. 53, no. 6, pp. 1130–1137, Jun. 2006.

[95] A. Novell and A. Bouakaz, "Chirp reversal power modulation contrast imaging," in *Proc. IEEE Int. Ultrason. Symp.*, Oct. 2011, pp. 632–635.

[96] A. Novell, S. Van Der Meer, M. Versluis, N. De Jong, and A. Bouakaz, "Contrast agent response to chirp reversal: Simulations, optical observations, and acoustical verification," *IEEE Trans. Ultrason., Ferroelectr., Freq. Control*, vol. 56, no. 6, pp. 1199–1206, Jun. 2009.

[97] M. Pasovic et al., "Second harmonic inversion for ultrasound contrast harmonic imaging," *Phys. Med. Biol.*, vol. 56, no. 11, pp. 3163–3180, 2011, doi: 10.1088/0031-9155/56/11/001.

[98] G. Renaud et al., "Counter-propagating wave interaction for contrast-enhanced ultrasound imaging," *Phys. Med. Biol.*, vol. 57, no. 21, pp. L9–L18, Nov. 2012.

[99] G. Renaud, J. G. Bosch, A. F. W. van der Steen, and N. de Jong, "Increasing specificity of contrast-enhanced ultrasound imaging using the interaction of quasi counter-propagating wavefronts: A proof of concept," *IEEE Trans. Ultrason., Ferroelectr., Freq. Control*, vol. 62, no. 10, pp. 1768–1778, Oct. 2015.

[100] F. S. Foster, P. N. Burns, D. H. Simpson, S. R. Wilson, D. A. Christopher, and D. E. Goertz, "Ultrasound for the visualization and quantification of tumor microcirculation," *Cancer Metastasis Rev.*, vol. 19, nos. 1–2, pp. 131–138, 2000.

[101] K. Wei, A. R. Jayaweera, S. Firoozan, A. Linka, D. M. Skyba, and S. Kaul, "Quantification of myocardial blood flow with ultrasound-induced destruction of microbubbles administered as a constant venous infusion," *Circulation*, vol. 97, no. 5, pp. 473–483, Feb. 1998.

[102] R. E. Pollard et al., "Contrast-assisted destruction-replenishment ultrasound for the assessment of tumor microvasculature in a rat model," *Technol. Cancer Res. Treatment*, vol. 1, no. 6, pp. 459–470, Dec. 2002.

[103] S. Feingold, R. Gessner, I. M. Guracar, and P. A. Dayton, "Quantitative volumetric perfusion mapping of the microvasculature using contrast ultrasound," *Investigative Radiol.*, vol. 45, no. 10, pp. 669–674, Oct. 2010.

[104] R. Williams et al., "Dynamic microbubble contrast-enhanced U.S. to measure tumor response to targeted therapy: A proposed clinical protocol with results from renal cell carcinoma patients receiving antiangiogenic therapy," *Radiology*, vol. 260, no. 2, pp. 581–590, Aug. 2011.

[105] P. N. Burns and H. Becher, "Contrast agents for echocardiography: Principles and instrumentation," in *Handbook of Contrast Echocardiography*, 2000, pp. 1–44.

[106] E. Barlow and A. J. Mulholland, "A fractional Fourier transform analysis of a bubble excited by an ultrasonic chirp," *J. Acoust. Soc. Amer.*, vol. 130, no. 5, pp. 3264–3270, Nov. 2011, doi: 10.1121/1.3626139.

[107] D. M. J. Cowell and S. Freear, "Separation of overlapping linear frequency modulated (LFM) signals using the fractional Fourier transform," *IEEE Trans. Ultrason., Ferroelectr., Freq. Control*, vol. 57, no. 10, pp. 2324–2333, Oct. 2010.

[108] S. Harput, J. McLaughlan, D. M. Cowell, and S. Freear, "Superharmonic imaging with chirp coded excitation: Filtering spectrally overlapped harmonics," *IEEE Trans. Ultrason., Ferroelectr., Freq. Control*, vol. 61, no. 11, pp. 1802–1814, Nov. 2014, doi: 10.1109/TUFFC.2014.006424.

[109] P. Phukpattaranont and E. S. Ebbini, "Post-beamforming second-order Volterra filter for pulse-echo ultrasonic imaging," *IEEE Trans. Ultrason., Ferroelectr., Freq. Control*, vol. 50, no. 8, pp. 987–1001, Aug. 2003.

[110] J. Du, D. Liu, and E. S. Ebbini, "Nonlinear imaging of microbubble contrast agent using the Volterra filter: *In vivo* results," *IEEE Trans. Ultrason., Ferroelectr., Freq. Control*, vol. 63, no. 12, pp. 2069–2081, May 2016.

[111] L. Demi, R. J. G. van Sloun, H. Wijkstra, and M. Mischi, "Cumulative phase delay imaging for contrast-enhanced ultrasound tomography," *Phys. Med. Biol.*, vol. 60, no. 21, pp. L23–L33, Nov. 2015.

[112] L. Demi, H. Wijkstra, and M. Mischi, "Cumulative phase delay between second harmonic and fundamental components—A marker for ultrasound contrast agents," *J. Acoust. Soc. Amer.*, vol. 136, no. 6, pp. 2968–2975, Dec. 2014.

[113] C. Tremblay-Darveau et al., "The role of microbubble echo phase lag in multipulse contrast-enhanced ultrasound imaging," *IEEE Trans. Ultrason., Ferroelectr., Freq. Control*, vol. 65, no. 8, pp. 1389–1401, Aug. 2018.

[114] M. Tanter, J.-L. Thomas, F. Coulouvrat, and M. Fink, "Breaking of time reversal invariance in nonlinear acoustics," *Phys. Rev. E, Stat. Phys. Plasmas Fluids Relat. Interdiscip. Top.*, vol. 64, no. 1, pp. 1–10, Jun. 2001.

[115] O. Couture, J. F. Aubry, G. Montaldo, M. Tanter, and M. Fink, "Tissue harmonics cancellation using time-reversal," in *Proc. IEEE Ultrason. Symp.*, Oct. 2008, pp. 1104–1107.

[116] M. F. Hamilton and D. T. Blackstock, *Nonlinear Acoustics*, 2008.

[117] E. B. Herbst, S. Unnikrishnan, S. Wang, A. L. Klibanov, J. A. Hossack, and F. W. Mauldin Jr., "The use of acoustic radiation force decorrelation-weighted pulse inversion for enhanced ultrasound contrast imaging," *Invest. Radiol.*, vol. 52, no. 2, pp. 95–102, Feb. 2017, doi: 10.1097/RLI.0000000000000313.

[118] Y. Huang et al., "Contrast-enhanced ultrasound imaging based on bubble region detection," *Appl. Sci.*, vol. 7, no. 10, p. 1098, Oct. 2017.

[119] J. Ma et al., "Spectrum enhanced colour ultrasound (SECU) imaging," *Measurement*, vol. 154, Mar. 2020, Art. no. 107401.

[120] J. Voorneveld et al., "High-frame-rate contrast-enhanced ultrasound for velocimetry in the human abdominal aorta," *IEEE Trans. Ultrason., Ferroelectr., Freq. Control*, vol. 65, no. 12, pp. 2245–2254, Dec. 2018.

[121] P. Song et al., "Notice of removal: Robust ultrasound super-resolution microvessel imaging with spatiotemporal nonlocal means filtering and bipartite graph-based microbubble tracking," in *Proc. IEEE Int. Ultrason. Symp. (IUS)*, Sep. 2017, pp. 149–167.

[122] K. Ito et al., "High-accuracy ultrasound contrast agent detection method for diagnostic ultrasound imaging systems," *Ultrasound Med. Biol.*, vol. 41, no. 12, pp. 3120–3130, Dec. 2015.

[123] A.-H. Liao, C.-C. Shen, and P.-C. Li, "Potential contrast improvement in ultrasound pulse inversion imaging using EMD and EEMD," *IEEE Trans. Ultrason., Ferroelectr., Freq. Control*, vol. 57, no. 2, pp. 317–326, Feb. 2010.

[124] U. R. Acharya et al., "Automated diagnosis of focal liver lesions using bidirectional empirical mode decomposition features," *Comput. Biol. Med.*, vol. 94, pp. 11–18, Mar. 2018.

[125] A. Y. Park and B. K. Seo, "Up-to-date Doppler techniques for breast tumor vascularity: Superb microvascular imaging and contrast-enhanced ultrasound," *Ultrasonography*, vol. 37, no. 2, pp. 98–106, Apr. 2018.

[126] Y. Desailly, A.-M. Tissier, J.-M. Correas, F. Wintzenrieth, M. Tanter, and O. Couture, "Contrast enhanced ultrasound by real-time spatiotemporal filtering of ultrafast images," *Phys. Med. Biol.*, vol. 62, no. 1, pp. 31–42, Jan. 2017.

[127] M. Bruce et al., "High-frequency nonlinear Doppler contrast-enhanced ultrasound imaging of blood flow," *IEEE Trans. Ultrason., Ferroelectr., Freq. Control*, vol. 67, no. 9, pp. 1776–1784, Sep. 2020.

[128] C. Tremblay-Darveau, R. Williams, L. Milot, M. Bruce, and P. N. Burns, "Combined perfusion and Doppler imaging using plane-wave nonlinear detection and microbubble contrast agents," *IEEE Trans. Ultrason., Ferroelectr., Freq. Control*, vol. 61, no. 12, pp. 1988–2000, Dec. 2014.

[129] K. Christensen-Jeffries, R. J. Browning, M.-X. Tang, C. Dunsby, and R. J. Eckersley, "In vivo acoustic super-resolution and super-resolved velocity mapping using microbubbles," *IEEE Trans. Med. Imag.*, vol. 34, no. 2, pp. 433–440, Feb. 2015.

[130] C. Errico et al., "Ultrafast ultrasound localization microscopy for deep super-resolution vascular imaging," *Nature*, vol. 527, no. 7579, pp. 499–502, Nov. 2015.

[131] P. Song, A. Manduca, J. D. Trzasko, R. E. Daigle, and S. Chen, "On the effects of spatial sampling quantization in super-resolution ultrasound microvessel imaging," *IEEE Trans. Ultrason., Ferroelectr., Freq. Control*, vol. 65, no. 12, pp. 2264–2276, Dec. 2018.

[132] S. Harput et al., "Two-stage motion correction for super-resolution ultrasound imaging in human lower limb," *IEEE Trans. Ultrason., Ferroelectr., Freq. Control*, vol. 65, no. 5, pp. 803–814, May 2018.

[133] T. Opacic et al., "Motion model ultrasound localization microscopy for preclinical and clinical multiparametric tumor characterization," *Nature Commun.*, vol. 9, no. 1, pp. 1–13, Apr. 2018.

[134] O. Couture, B. Besson, G. Montaldo, M. Fink, and M. Tanter, "Microbubble ultrasound super-localization imaging (MUSLI)," in *Proc. IEEE Int. Ultrason. Symp.*, Oct. 2011, pp. 1285–1287.

[135] M. Siepmann, G. Schmitz, J. Bzyl, M. Palmowski, and F. Kiessling, "Imaging tumor vascularity by tracing single microbubbles," *IEEE Int. Ultrason. Symp. IUS*, pp. 1906–1908, 2011.

[136] K. Christensen-Jeffries et al., "Super-resolution ultrasound imaging," *Ultrasound Med. Biol.*, vol. 46, no. 4, p. 865, Apr. 2020.

[137] S. B. Andersen et al., "Super-resolution imaging with ultrasound for visualization of the renal microvasculature in rats before and after renal ischemia: A pilot study," *Diagnostics*, vol. 10, no. 11, pp. 1–15, 2020.

[138] D. Ghosh, F. Xiong, S. R. Sirsi, P. W. Shaul, R. F. Mattrey, and K. Hoyt, "Toward optimization of *in vivo* super-resolution ultrasound imaging using size-selected microbubble contrast agents," *Med. Phys.*, vol. 44, no. 12, pp. 6304–6313, Dec. 2017.

[139] Y. Desailly, O. Couture, M. Fink, and M. Tanter, "Sono-activated ultrasound localization microscopy," *Appl. Phys. Lett.*, vol. 103, no. 17, Oct. 2013, Art. no. 174107.

[140] M. A. O'Reilly and K. Hynynen, "A super-resolution ultrasound method for brain vascular mapping," *Med. Phys.*, vol. 40, no. 11, Oct. 2013, Art. no. 110701.

[141] K. G. Brown and K. Hoyt, "Evaluation of nonlinear contrast pulse sequencing for use in super-resolution ultrasound imaging," *IEEE Trans. Ultrason., Ferroelectr., Freq. Control*, vol. 68, no. 11, pp. 3347–3361, Nov. 2021.

[142] A. Bar-zion, C. Tremblay-darveau, O. Solomon, D. Adam, and Y. C. Eldar, "Spatial resolution and background rejection," *IEEE Trans. Med. Imag.*, vol. 36, no. 1, pp. 169–180, Oct. 2017.

[143] K. C. Jeffries et al., "Notice of removal: Microbubble localization errors in ultrasonic super-resolution imaging," in *Proc. IEEE Int. Ultrason. Symp. (IUS)*, Sep. 2017, pp. 1644–1654.

[144] D. Ackermann and G. Schmitz, "Detection and tracking of multiple microbubbles in ultrasound B-mode images," *IEEE Trans. Ultrason., Ferroelectr., Freq. Control*, vol. 63, no. 1, pp. 72–82, Jan. 2016.

[145] M. J. Rust, M. Bates, and X. Zhuang, "Sub-diffraction-limit imaging by stochastic optical reconstruction microscopy (STORM)," *Nature Methods*, vol. 3, no. 10, pp. 793–795, 2006, doi: 10.1038/nmeth929.

[146] R. J. G. van Sloun, O. Solomon, M. Bruce, Z. Z. Khaing, Y. C. Eldar, and M. Mischi, "Deep learning for super-resolution vascular ultrasound imaging," in *Proc. IEEE Int. Conf. Acoust., Speech Signal Process. (ICASSP)*, May 2019, pp. 1055–1059.

[147] X. Liu, T. Zhou, L. Mengyang, Y. Yang, Q. He, and J. Luo, "Deep learning models for fast ultrasound localization microscopy," in *Proc. IEEE Int. Ultrason. Symp. (IUS)*, Sep. 2020, pp. 3064–3078.

[148] K. G. Brown, D. Ghosh, and K. Hoyt, "Deep learning of spatiotemporal filtering for fast super-resolution ultrasound imaging," *IEEE Trans. Ultrason., Ferroelectr., Freq. Control*, vol. 67, no. 9, pp. 1820–1829, Sep. 2020.

[149] *Contrast Enhanced Ultrasound Market Size Report, 2021–2028*, Grand View Research, Pune, India, 2021.

[150] R. G. Barr, "Off-label use of ultrasound contrast agents for abdominal imaging in the United States," *J. Ultrasound Med.*, vol. 32, no. 1, pp. 7–12, Jan. 2013.

[151] D. Hyun, L. Abou-Elkacem, V. A. Perez, S. M. Chowdhury, J. K. Willmann, and J. J. Dahl, "Improved sensitivity in ultrasound molecular imaging with coherence-based beamforming," *IEEE Trans. Med. Imag.*, vol. 37, no. 1, pp. 241–250, Jan. 2018.

[152] J. Viti, H. J. Vos, N. D. Jong, F. Guidi, and P. Tortoli, "Detection of contrast agents: Plane wave versus focused transmission," *IEEE Trans. Ultrason., Ferroelectr., Freq. Control*, vol. 63, no. 2, pp. 203–211, Feb. 2016.

[153] O. Couture, M. Fink, and M. Tanter, "Ultrasound contrast plane wave imaging," *IEEE Trans. Ultrason., Ferroelectr., Freq. Control*, vol. 59, no. 12, pp. 2676–2683, Dec. 2012.

[154] Y. Zhang and A. Demosthenous, "Integrated circuits for medical ultrasound applications: Imaging and beyond," *IEEE Trans. Biomed. Circuits Syst.*, vol. 15, no. 5, pp. 838–858, Oct. 2021.

[155] K. Sun et al., "A 180-Vpp integrated linear amplifier for ultrasonic imaging applications in a high-voltage CMOS SOI technology," *IEEE Trans. Circuits Syst. II, Exp. Briefs*, vol. 62, no. 2, pp. 149–153, Feb. 2015.
[156] Z. Gao, P. Gui, and R. Jordanger, "An integrated high-voltage low-distortion current-feedback linear power amplifier for ultrasound transmitters using digital predistortion and dynamic current biasing techniques," *IEEE Trans. Circuits Syst. II, Exp. Briefs*, vol. 61, no. 6, pp. 373–377, Jun. 2014.
[157] D. Bianchi, F. Quaglia, A. Mazzanti, and F. Svelto, "Analysis and design of a high voltage integrated class-B amplifier for ultra-sound transducers," *IEEE Trans. Circuits Syst. I, Reg. Papers*, vol. 61, no. 7, pp. 1942–1951, Jul. 2014.
[158] D. Ghisu, A. Gambero, M. Terenzi, G. Ricotti, A. Moroni, and S. Rossi, "180 Vpp output voltage, 24 MHz bandwidth, low power class AB current-feedback high voltage amplifier for ultrasound transmitters," in *Proc. IEEE Custom Integr. Circuits Conf. (CICC)*, Apr. 2018, pp. 1–4.
[159] R. J. G. van Sloun et al., "Super-resolution ultrasound localization microscopy through deep learning," *IEEE Trans. Med. Imag.*, vol. 40, no. 3, pp. 829–839, Mar. 2021.
[160] K. G. Brown, S. C. Waggener, A. D. Redfern, and K. Hoyt, "Faster super-resolution ultrasound imaging with a deep learning model for tissue decluttering and contrast agent localization," *Biomed. Phys. Eng. Exp.*, vol. 7, no. 6, Oct. 2021, Art. no. 065035.

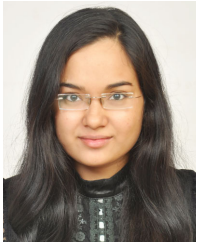

SAPNA R. BISHT received the B.E. and M.E. degrees in biomedical engineering from Gujarat Technological University, India. She is currently pursuing the Ph.D. degree in biological engineering at the Indian Institute of Technology Gandhinagar, India, focused on ultrasound elastography.

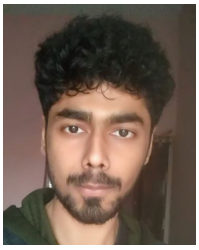

VISHWAS V. TRIVEDI received the bachelor's degree in electronics and communication engineering from Charotar University and the master's degree in signal processing from the Dhirubhai Ambani Institute of Information and Communication Technology. He is currently pursuing the Ph.D. degree in electrical engineering at IIT Gandhinagar, India. His research interests include therapeutic ultrasound image guidance.

ROHIT BHARDWAJ received the bachelor's degree from the Sri Sai College of Engineering and Technology, India, and the master's degree from the National Institute of Technical Teacher's Training and Research in 2010. He was a Research Assistant with the Thapar Institute of Engineering and Technology, India, until Spring 2022.

CHANDAN K. JHA received the bachelor's degree in biomedical engineering from the National Institute of Technology Raipur, India, and the Ph.D. degree in electrical engineering from IIT Gandhinagar, India. He was a Post-Doctoral Fellow in electrical engineering with IIT Gandhinagar until October 2022. His research interests include optical and ultrasonic sensing.

DEBABRATA GHOSH (Member, IEEE) received the B.E. degree in electronics and instrumentation engineering from Vidyasagar University, India, the M.Sc. degree in satellite communication and space systems from the University of Sussex, U.K., and the Ph.D. degree in electrical engineering from the University of North Dakota, USA. From 2016 to 2018, he was a Post-Doctoral Researcher with the Radiology Department, UT Southwestern Medical Center, USA, and also with the Bioengineering Department, The University of Texas at Dallas, USA. Since 2018, he has been an Assistant Professor in electronics and communication engineering at the Thapar Institute of Engineering and Technology, India. His research interests include new imaging algorithms for ultrasound.

HIMANSHU SHEKHAR (Senior Member, IEEE) received the Ph.D. degree from the University of Rochester and he completed postdoctoral training from the University of Cincinnati. He is currently an Assistant Professor in electrical engineering with the Indian Institute of Technology Gandhinagar, India. His research interests include ultrasound-mediated therapy, molecular imaging, and sensing. His work has been recognized with the F. V. Hunt Post-Doctoral Fellowship, the Har Govind Korana Innovative Young Biotechnologist Award, and the Star Ambassador Lectureship Award from the IEEE UFFC Society. He serves on the Technical Committees of Biomedical Acoustics for the Acoustical Society of America, IEEE International Ultrasonics Symposium, and Chairs the Professional Networking and Mentoring Committee of the IEEE UFFC Society.